Modified Inductive Multi-Coil Wireless Power Transfer Approach Based On Z-Source Network

Bohdan Pakhaliuk, *Student Member, IEEE*, Oleksandr Husev, *Senior Member, IEEE*, Viktor Shevchenko, *Student Member, IEEE*, Janis Zakis, *Senior Member, IEEE,* Maksym Khomenko, Ryszard Strzelecki, *Senior Member, IEEE*

Abstract— **This article presents a non-conventional approach to a multi-coil wireless power transfer system based on a Z-source network. The novelty of the approach lies in the use of a Z-source as a voltage source for energy transmission through the wireless power transfer coils. The main advantage is in a reduced number of semiconductors. This paper provides the design approach, simulation and experimental study. Feasibility and possible application fields are presented in the conclusions.**

Index Terms— **Wireless charging, inductive charging, Z-source network, coupled coils**

I. INTRODUCTION

Wireless power transfer technology is becoming more popular [1]-[12]. Its maintainability and safety give a new dimension to the development of electronic equipment. The field of application is wide. Low power chargers are used in household appliances like toothbrushes or phones. Also, non-invasive pacemaker charging systems make use of the technology [13]-[15], whereas invasive operations can be eliminated. High power chargers are used for charging electric cars [16]-[23], buses and boats [24]-[27].

There are different ways to transmit the energy by wireless: by using a capacitive coupling [28], [29], inductive coupling [30]-[33], [36], resonant inductive coupling, sound waves, microwaves, and light waves. Wireless power transfer based on the capacitive and inductive coupling is most popular. The capacitive power transfer is mostly used for low power applications, whereas an inductive coupling can be used for low and high power and with an air gap relatively larger than in the capacitive approach.

International standards like Qi [34],[35] allow for the development of devices compatible with the wireless charging systems all over the world. They specify the working frequency range, the output power, and communication link types. Special standards are also provided to incr1ease the safety of devices by satisfying devices with an electromagnetic field. They provide ways of overcoming the electromagnetic influence on people, such as reducing power or involving additional coils shielding. On the other hand, the presence of coupled coils with a comparably large air gap provides additional tasks to be solved using this technology. The air gap between the transmitter and the receiver coils increases rapidly the leakage inductance and leads to increasing losses. In this case, high power system development is a challenging task [36]. Different approaches can be used to increase the system performance. In one of the approaches, high-quality elements like capacitors with low equivalent series resistance and transistors with a low R_{dson} are used in the inverter. Using this method, the losses in the inverter and the wireless power transfer part can be reduced. However, the price of the final device can dramatically increase, which will limit its application to specific fields. The second approach is mostly concerned with the design of the coils, adding a ferrite material to concentrate the flux and increase the coupling coefficient or using the litz wires to reduce the skin and proximity effects. The aim is to increase the coil's quality factor. As it was shown in [37], Figure-of-Merit FoM = kQ limits the efficiency to $\eta = FoM^2/(1+\sqrt{1+FoM^2})^2$, where k is a coupling coefficient and Q is a quality factor. Accordingly, in commonly used solutions, the transmitter and the receiver coils are situated between two ferrite plates or pot-cores. In this case, the flux is concentrated between them and as a result, the coupling coefficient can be effectively increased. The third approach uses multicoil solutions [1], [7], [38]-[48]. In this approach, an effective area where high efficiency is obtained can be rapidly

increased. The system can maintain high performance for significant transmitting and receiving coils misalignment whereas the efficiency of the two coils solution with the same misalignment will decrease dramatically. A popular approach is maximum efficiency tracking, which can be implemented by changing the switching frequency [49], [50], the impedance [51], the load or other parameters to adapt to the system changes (like air gap), to match the load and correspondingly find the point with the highest efficiency. Unlike other approaches, this solution needs additional sensors (and sometimes communication links between the transmitter and the receiver) to estimate an optimal point.
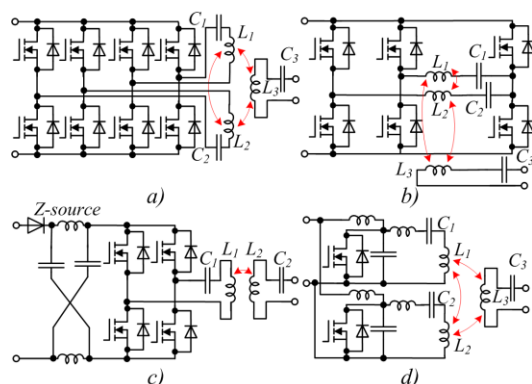

Fig. 1. Existing IPT solutions: (a) with eight transistors; (b) with six transistors; (c) with Z-source network; (d) with E-class inverter.

Commonly, multicoil solutions use wireless power transfer topologies based on the full-bridge [38] and half-bridge circuits [44] shown in Fig. 1a and Fig. 1b, respectively. The advantages of such approaches are full controlability of each transmitting coil (coils can work separately or simultaneously, with a phase shift or without) and possibility to implement various control methods like phase-shifted control [38] or input power splitting [41], where an optimal amount of transmitted power is chosen for each coil to maintain high efficiency at variable lateral misalignment. As can be seen, the inverter topologies with two transmitting coils are utilizing eight and six switches. This increases the control complexity and the dimensions along with an increasing price. Topologies based on an E-class inverter are also used (Fig. 1d). They combine simplicity and ability to work in the ZVS and ZDS mode. The disadvantage is based on high voltage stress on the semiconductor elements, which can be up to 3.5 times higher than the input DC voltage [52]. To implement two transmitters, it is necessary to have two switching elements.

The purpose of this work is to improve the WPT systems in terms of power density and complexity. This paper proposes a novel topology that lacks drawbacks of conventional topologies based on the full- or half-bridge circuitry. By using the inverter based on the Z-source network, a rapid decrease in the number of active elements can be achieved along with increased reliability. This enables reduction in the size and price of the system. Multiple transmitting coils allow for different designs to be created by changing the misalignment between the transmitting coils. A new dimension of freedom provides for increased density of the flux or increased transmitted area. On the other hand, the disadvantages of the proposed solution are

related to the limited system controllability. The topology cannot control each transmitting coil independently, as only one control element is available in the circuit. The advantage of the converters based on the Z-source is that the Z-source network can work in both the buck and the boost mode, which is impossible in conventional solutions [53]. As the switching elements are connected to the supply through the Z-source inductors, the topology is not suffering from the noise misgating-on effect. By overcoming this disadvantage, the reliability can be increased and the damage of the active elements at simultaneous switch-on of both the low and high side transistors can be prevented. A Z-source was already used in WPT applications in its conventional implementation (Fig. 1c) [54]-[57]. Each solution has additional features like PFC and inverter operations implemented only by the Z-source network [54] or using asymmetrical voltage-cancellation control to increase the efficiency and perform ZVS operation modes [55]. In total, these solutions use at least four switching elements in inductive power transfer systems for one transmitting coil and in current solutions, only one transmitter limits its applications mostly in static charging where the low variation of the air gap is expected to be in the working mode.

The article is divided into three main sections. Section II explains the operation principle of the proposed topology and its operation modes. Also, it contains guidelines for component estimation for different transmitter coil positions. Section III is devoted to the simulation study where the expected operation principle is verified along with the simulations for different operation conditions. In section IV, the developed experimental setup of the proposed topology is experimentally investigated in different operation conditions: for different transmitter coils positions, loads, switching frequencies, misalignments between the receiver and the transmitter and also for topologies with different blocking elements. Finally, in the temperature analysis, the solutions are compared with a blocking element represented by a diode and a transistor.

II. DESCRIPTION OF OPERATION PRINCIPLE AND COMPONENT DESIGN

The proposed IPT solution is shown in Fig. 2. It consists of four parts: an inverter (1), transmitting coil with the compensation (2), receiving coil with the compensation (3), and rectifier part (4). The inverter is based on the Z-source network [58]-[60]. It consists of passive elements: two capacitors, two inductors and two active elements. In this topology, the transistor T_2 is used as a switch to transform the topology between two series (C_{z1}, L_{z2} and C_{z2}, L_{z1}) and two parallel (C_{z1}, L_{z1} and C_{z2}, L_{z2}) resonant circuits. In the boost mode, the voltages obtained on the reactive elements of the Z-source network are higher than the input voltage. To prevent this voltage passing to the voltage source, the diode D_1 or the transistor T_1 (Fig. 2) is used. As can be seen, the transistors work in a complementary mode. The second and third parts (Fig. 2) are represented by the transmitting and receiving coils along with the compensation capacitors. The capacitors are used to reduce the influence of a high leakage inductance based on a

higher air gap than in a regular transformer and as a result, they increase the system efficiency.

The compensation capacitor can be connected in series or in parallel, depending on the demanded voltage and current. This provides four combinations: series-series, series-parallel, parallel-series, and parallel-parallel. The commonly used types of compensation are series-series and series-parallel. For low power applications, they are mostly preferable as they utilize the lowest amount of copper, which decreases the size and price of coils. As the variation of lateral displacement is addressed in this work, series-series compensation was considered as the optimal solution. The reason is that in this case, a variation of the coupling coefficient corresponds only to the variation of the reflected resistance and there is no variation of reactance. So the system appears to work in the resonant mode without reactive currents in all possible modes, which is impossible for series-parallel compensation without additional compensation elements or additional optimal tracking.
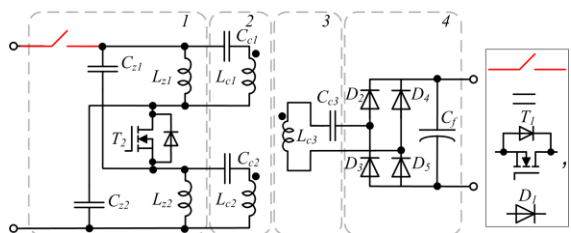

Fig. 2.   The proposed solution for the IPT based on a Z-source network.

As can be seen from the structure of the proposed solution, it can be divided into two main parts. The first one is the Z-source network, which plays the role of the voltage generator, and the second part consists of the transmitting and receiving coils along with the secondary-side rectifier.

A. Z-source network design

The reactive elements of the Z-source network in their regular applications are tuned to a resonance frequency much lower than the switching frequency to reduce pulsations [53]. In this case, these elements are also working like a second-order low pass filter. In this work, elements of a z-source network are tuned commensurate to have resonance for half of the switching frequency. Then the quasi-sinusoidal voltages can be obtained on the Z-source inductors. The ideal diagrams of the expected voltages obtained on the Z-source network for equal coupling coefficients k_{13} and k_{23} are shown in Fig. 3. For the solutions with two transistors, the dead-time should be involved between the switching transitions. Without the dead-time, the Z-source network inductors can be shorted to the power source and it leads to transmitting signal distortion and rapid decrease of the transmitted power. In the case of ideal compensation on the secondary and the primary sides, the IPT part can be represented by an equivalent resistor R_{eq}. The capacitor value can be calculated from the conventional resonance equation (1) by only taking into consideration the half-switching frequency:

$$C_{z1,z2}=1/((\omega/2)^2 L_{z1,z2});\qquad(1)$$

The equivalent circuits for three states of the topology are shown in Fig. 3.
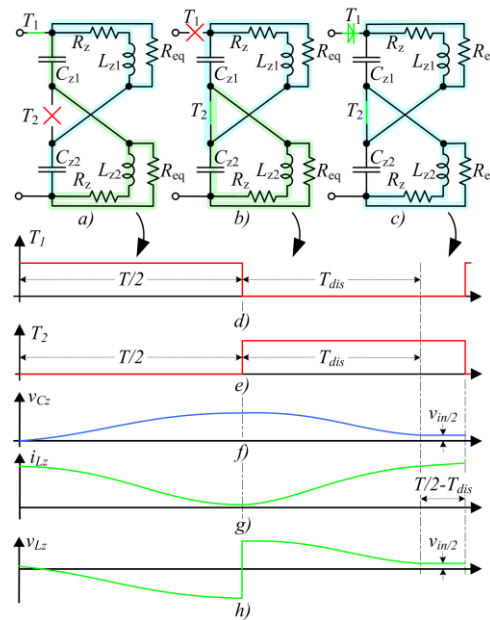

Fig. 3.   Equivalent circuits of a Z-source based IPT: (a) at the transistor turn-off; (b) at the transistor turn-on; (c) at the transistor turn-on and the capacitors discharge to $v_{in}/2$; (d) Transistor T_1 state; (e) Transistor T_2 state; (f) Capacitors C_{z1} and C_{z2} voltages (g) Inductors L_{z1} and L_{z2} currents; (h) Inductors L_{z1} and L_{z2} voltages.

When the transistor T_2 is turned off and the transistor T_1 is turned on (Fig. 3a), the input voltage charges the capacitors. Equations expressing the first state are as follows:

$$
\begin{cases}
v_{in} = v_{c_{z2}}^{(1)}(t) + L_{z1}\dfrac{di_{L_{z1}}^{(1)}(t)}{dt} + i_{L_{z1}}^{(1)}(t)\cdot R_z \\[2ex]
v_{in} = v_{c_{z1}}^{(1)}(t) + L_{z2}\dfrac{di_{L_{z2}}^{(1)}(t)}{dt} + i_{L_{z2}}^{(1)}(t)\cdot R_z \\[2ex]
C_{z1}\dfrac{dv_{C_{z1}}^{(1)}(t)}{dt} = i_{L_{z2}}^{(1)}(t) + \dfrac{L_{z2}}{R_{eq}}\dfrac{di_{L_{z2}}^{(1)}(t)}{dt} \\[2ex]
C_{z2}\dfrac{dv_{C_{z2}}^{(1)}(t)}{dt} = i_{L_{z1}}^{(1)}(t) + \dfrac{L_{z1}}{R_{eq}}\dfrac{di_{L_{z1}}^{(1)}(t)}{dt}
\end{cases}\cdot\qquad(2)
$$

When the transistor T_2 is turned on, the topology is transformed to the two parallel resonant circuits (Fig. 3b) and the charge on the capacitors is being discharged on the inductors. Equations expressing the second state are:

$$
\begin{cases}
v_{C_{z1}}^{(2)}(t) = L_{z1}\dfrac{di_{L_{z1}}^{(2)}(t)}{dt} + i_{L_{z1}}^{(2)}(t)\cdot R_z \\[2ex]
v_{C_{z2}}^{(2)}(t) = L_{z2}\dfrac{di_{L_{z2}}^{(2)}(t)}{dt} + i_{L_{z2}}^{(2)}(t)\cdot R_z \\[2ex]
-C_{z1}\dfrac{dv_{C_{z1}}^{(2)}(t)}{dt} = i_{L_{z1}}^{(2)}(t) + \dfrac{L_{z1}}{R_{eq}}\dfrac{di_{L_{z1}}^{(2)}(t)}{dt} \\[2ex]
-C_{z2}\dfrac{dv_{C_{z2}}^{(2)}(t)}{dt} = i_{L_{z2}}^{(2)}(t) + \dfrac{L_{z2}}{R_{eq}}\dfrac{di_{L_{z2}}^{(2)}(t)}{dt}
\end{cases}\cdot\qquad(3)
$$

It should be noted that the topology will switch to the next state at the moment $T/2+T_{dis}$. Discharge time T_{dis} can be evaluated from the next expression and its value is in a range $0..T/2$:

$$v_{C_{z1}}{}^{(2)}(t) = v_{in}/2 \,. \qquad (4)$$

In the third state (Fig. 3c), while the transistor T_1 is closed, its body diode starts to conduct and the current passes through the inductors and equivalent load. As the capacitors are charged to the half of the input voltage, no current is passing the capacitors. Equations representing the third state are shown below:

$$
\begin{cases}
v_{in} = L_{z1}\dfrac{di_{L_{z1}}{}^{(3)}(t)}{dt} + L_{z2}\dfrac{di_{L_{z2}}{}^{(3)}(t)}{dt} + \\[2mm]
\quad + i_{L_{z1}}{}^{(3)}(t)\cdot R_z + i_{L_{z2}}{}^{(3)}(t)\cdot R_z \\[2mm]
i_{L_{z1}}{}^{(3)}(t) + \dfrac{L_{z1}}{R_{eq}}\dfrac{di_{L_{z1}}{}^{(3)}(t)}{dt} = i_{L_{z2}}{}^{(3)}(t) + \dfrac{L_{z2}}{R_{eq}}\dfrac{di_{L_{z2}}{}^{(3)}(t)}{dt} \\[2mm]
C_{z1}\dfrac{dv_{C_{z1}}{}^{(3)}(t)}{dt} = 0 \\[2mm]
C_{z2}\dfrac{dv_{C_{z2}}{}^{(3)}(t)}{dt} = 0
\end{cases} \quad . \ (5)
$$

To obtain a mathematical model for one switching period, differential equations were solved for capacitor voltages and inductor currents. These solutions involve unknown constants of integration. The constants can be evaluated by merging the boundary conditions for the system in the steady-state mode by solving a system where the start condition of the state is equalized to the final condition of the previous state. Finally, by evaluating constants of integration, currents in the inductors (and similarly, capacitor voltages) for one switching period can be obtained by merging all states with the Heaviside function. Due to bulkiness, these equations are not shown in this paper. The power obtained on the equivalent resistors can be acquired from the inductor current. This power can be recalculated to obtain the output power and estimate the losses.

B. Application of multiple coupled coils

The design of the multiple coupled coils is presented in Figs. 4a and 4b. It consists of two transmitting coils with a 100% and 50% intersection and a receiving coil. The reason for such choice is that the first design is expected to increase the efficiency of the system as compared to solutions with one transmitting coil while in the second solution, the transmitted flux would rapidly be expanded on a larger area, increasing the tolerance to the misalignment.

To represent such coupled coil designs, two models can be used. The first one uses self-inductance of the coils and a mutual inductance between them [61]. The second model uses two leakage inductances, a magnetizing inductance and an ideal transformer to represent the turns ratio between the coupled inductors [62]. If the inductance of the coils is the same, the ideal transformer can be removed. In the cases of multicoil

solutions, the first model is preferred, as it can show all the relations between the coils in a simple way. A coupling coefficient is a relation between self-inductances and mutual inductances, which represent the amount of energy transferred from one coil to another. It can be estimated as $k = M/(\sqrt{L_1 L_2})$.
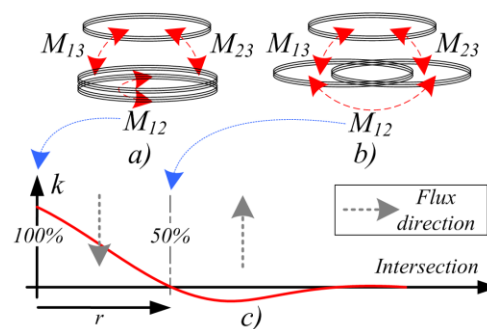

Fig. 4. Coils: (a) design with 100% intersection; (b) design with 50% intersection; (c) coupling value between two coils under different intersections.

It should be noted that in the first design, the coupling coefficient between the primary and the secondary side coils is significantly lower than that between the primary side coils, which is approaching 1. In the second design, the coupling between the primary coils is significantly (~10-40 times) lower than that between the primary and the secondary side. The relation between the coupling and two coils misalignment is shown in Fig. 4c. After 50% intersection, the flux is changing its direction because the inner space of the second coil is gathering more outer then inner flux of the first coil and vice versa. With such intersection, each transmitting coil can work independently.

C. IPT part design

The advantages of the series-series compensation lie in an arbitrary air gap compensation without the necessity of active matching. This can be done because the components are defined only by the working frequency. In this case, there is no need to maintain a constant coupling coefficient in an optimal point. The disadvantage is a load-dependent voltage transfer ratio for different coupling coefficients. In the case of a series-parallel compensation, the component parameters are additionally set to a fixed coupling coefficient, which corresponds to a fixed air gap between the coils.

This approach appears more suitable for the stationary systems where the air gap remains constant. For variable coupling, any deviation in the high side or the low side from the calculated coupling will lead to a decrease in the efficiency. Such an approach should be actively matched to be situated in the optimal point. Unlike a series-series compensation, this approach gives a load-independent voltage transfer ratio. This feature enables the elimination of the communication link between the primary and the secondary side and simplifies the final system. In this paper, the air gap is considered to be variable and series-series compensation is preferable. In this case, variable matching elements are not necessary, resulting in reduced system complexity.

The power received on the secondary side is rectified in the fourth part of the system by a diode rectifier. Also, to reduce

high frequency voltage pulsations, a filtering capacitor is necessary. The equivalent circuit of an IPT (inductive power transfer) part with all necessary parameters is shown in Fig. 5. To simplify the model, a bridge rectifier with the load was replaced by the equivalent ac resistor R_{Leq}. The value of this equivalent resistor is equal to the amount of the energy consumed by the load with the rectifier $R_{Leq}=(8/\pi^2)(V^2_{2,dc}/P_2)$.
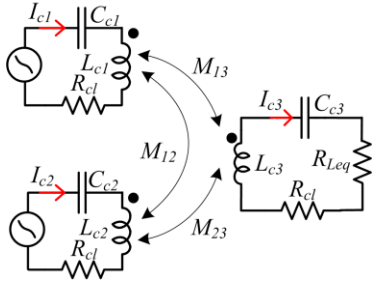
Fig. 5. Equivalent circuit representing the IPT topology.

To evaluate the compensation capacitors values (7), (9), the impedance on the primary side should be obtained along with the reflected impedances for both solutions (6), (8). For the first position when $M_{12}>M_{13}\approx M_{23}$, as can be seen, the reactive component to be compensated by the capacitor is $L_{c1}+M_{12}$:

$$Z_{1,2}=(2\omega^2 M^2_{13,23})/(R_{Leq}+R_{lc})+j\omega(L_{c1,c2}+M_{12}); \quad (6)$$

$$C_{c1,c2}=1/(\omega^2(L_{c1,c2}+M_{12})); \quad (7)$$

In the second situation when $M_{12}<<M_{13}\approx M_{23}$, the coupling coefficient between the primary side coils is low and M_{12} component can be neglected:

$$Z_{1,2}=(2\omega^2 M^2_{13,23})/(R_{Leq}+R_{lc})+j\omega L_{c1,c2}; \quad (8)$$

$$C_{c1,c2}=1/(\omega^2 L_{c1,c2}); \quad (9)$$

The equations obtained show that for $M_{13}\approx M_{23}$ in both situations, reflected impedance has no reactive components. Additionally, as compared to the solutions with one transmitter, number 2 appears in equations (6), (8), which indicates that the increase in the amount of the transmitting coils will increase the reflected impedance for each coil. The secondary side compensation capacitor is the same for both situations $C_{c3}=1/(\omega^2 L_{c3})$.

The results of the arbitrary displacement for both solutions in the first harmonic approximation with compensation are shown in Fig. 6. The compensation capacitors are involved in the simulation and are tuned accordingly to (7) and (9). Fig. 6a shows that in the first situation, the coupling between the transmitting and the receiving coils is changing equally and the corresponding mutual inductances are also equal, whereas in the second situation (Fig. 6b), the coupling coefficients and the corresponding mutual inductances are different. As Fig. 6c and Fig. 6d show, the compensation is effectively working on the whole range of the displacement whereas in the second simulation, the full compensation is obtained only for the zero displacement. This means that the second solution reflects a coupling dependent reactance to the primary side.
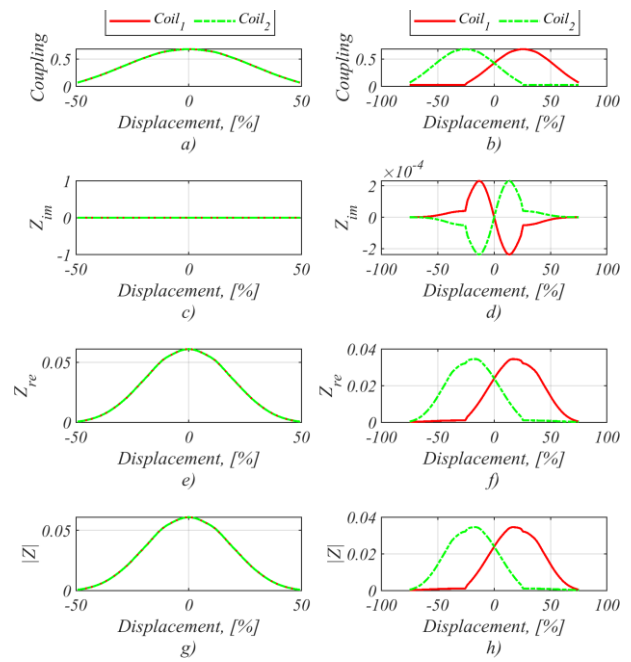

Fig. 6. First harmonic coils: (a) coupling coefficient for the first situation; (b) coupling coefficient for the second situation; (c) imaginary part Z_{im} for the first situation; (d) imaginary part Z_{im} for the second situation; (e) real part Z_{re} for the first situation; (f) real part Z_{re} for the second situation; (g) |Z| for the first situation; (h) |Z| for the second situation.

III. SIMULATION STUDY

The simulation was performed in a PSIM simulation environment. The parameters of the simulations are listed in Table 1. The model includes the losses in the components. For the chosen passive losses, the quality factor of the transmitting and the receiving coil can be $Q=\sim500$. The transistor drain source resistance R_{dson} is $3.5\ m\Omega$. As the low ESR capacitors are used, this parameter is neglected in the model.

The simulation in Fig. 7 shows the main voltages and currents of the topology.

TABLE I
SIMULATION PARAMETERS

| Parameter symbol	Appearance		
	Brief description	Value	Units
f_{sw}	Z-source switching frequency	140	kHz
L_{z1},L_{z2}	Z-source inductance	11	uH
C_{z1},C_{z2}	Z-source capacitance	470	nF
L_{c1},L_{c2}	Transmitting coil inductance	5.8	uH
C_{c1},C_{c2}	Primary side capacitance	222	nF
L_{c3}	Receiving coil inductance	5.8	uH
C_{c3}	Secondary side capacitance	222	nF
C_f	Filtering capacitor	1000	uF
R_L	Nominal load value	5	Ω
$R_z,$	Losses in inductances and	0.01	Ω
R_{cl}	wireless power transfer coils		
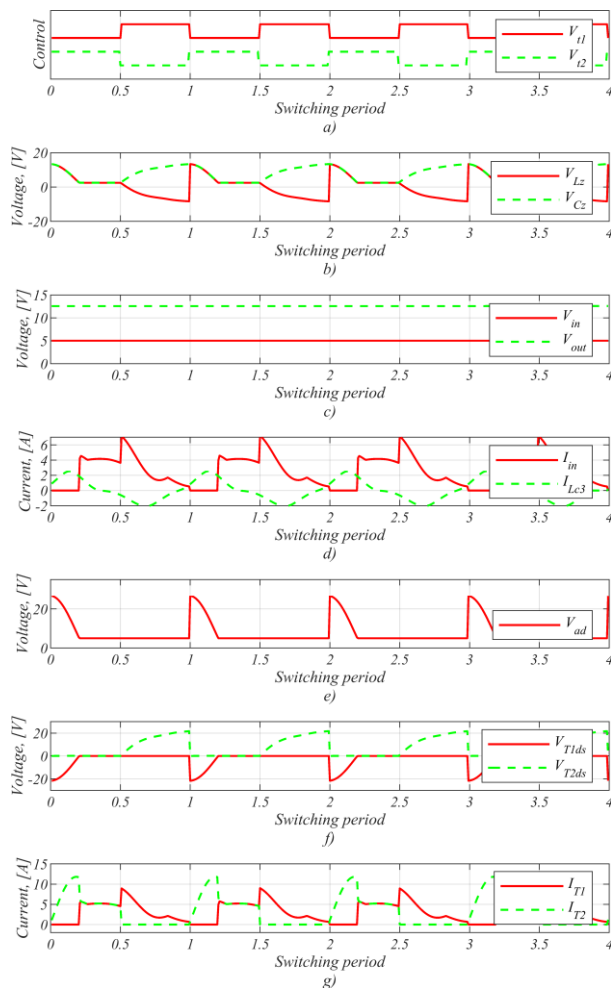
Fig. 7. Simulation results of the first solution: (a) control signals; (b) Z-source voltages; (c) output and input voltages; (d) input and receiving coil current; (e) voltage after blocking element; (f) transistors drain-source voltages; (g) transistors currents.

The input and output voltages are shown in Fig. 7c. It can be seen that the topology works in the boost mode and the output voltage is nearly twice higher than the input. The load voltage and current remain constant and can be used in the battery charging applications. The obtained inductor and capacitor voltages V_{Lz} and V_{Cz} of the Z-source network are shown in Fig. 7b. The received current obtained on the secondary side coil is shown in Fig. 7d. The non-sinusoidal shape is caused by the nonlinear load represented by the rectifier.

Fig. 7e shows that the blocking transistor works in a regular mode and when the voltage after the blocking transistor is higher than the input voltage, there is no current passing in the reverse direction (state 2).

As experimental measurements of currents and voltages across the transistors cannot be implemented without significant influence on the inverter work, we analyzed the measurements in the simulation study. Fig. 7f and Fig. 7g show that the transistor T_1 switches on under a ZVS condition and switches off under the Zero Current (ZCS) condition. T_2 is not switching under ZVS condition but ZCS is observed, while switches off under ZVS condition.

IV. EXPERIMENTAL STUDY

To verify the proposed topology and the coil designs, a wireless power transfer testing set (Fig. 8a) was developed. It consists of a control board, a converter board, coupled coils and the load.

As the main task was to verify the effectiveness of the topology, both primary and secondary sides were made on one PCB, and MOSFET transistors were chosen to simplify the system. In the commercial implementation, GaN transistors can be more preferable as the increase of efficiency and switching frequency can be implemented. Input voltage $V_{in}=5V$. The main parameters of the experimental setup are listed in Table 2.

Commercially available coils from Würth Elektronics were used. The coils are made with two litz wires connected in parallel and have ferrite plates to concentrate the flux. The transistor switching signals were generated by a development board with a microcontroller STM32F407VGT with the operation frequency 168 MHz.

The coils were mounted on a plastic holder to maintain a constant coupling in all modes. For correlation with the simulation, the study positions were chosen the same as was mentioned in section II (Fig. 8b - Fig. 8d). The experimental plots of the solution with the transistor for a few working periods are shown in Fig. 9. The voltages obtained on the Z-source components (Fig. 9a and Fig. 9e) are similar to the voltages obtained in the simulations. It should be noted that the high frequency oscillations present in a signal appear to be caused by the interactions between the drain-source output transistor capacitance and the z-source inductors.

TABLE II
EXPERIMENTAL PARAMETERS

| Parameter symbol	Appearance		
	Brief description	Value	Units
Primary side			
f_{sw}	Switching frequency	140	*kHz*
L_{z1},L_{z2}	Z-source inductance	11	*uH*
C_{z1},C_{z2}	Z-source capacitance	470	*nF*
IPT coils – 760308102142			
L_{c1},L_{c2},L_{c3}	Coil inductance	5.8	*uH*
R_{cl}	DC resistance	10	*mΩ*
Q	Quality factor	100	
Transistors - IPI041N12N3			
V_{DS}	Drain-source voltage	120	*V*
R_{DS}	Drain-source on-state resistance	3.5	*mΩ*
I_{DS}	Continuous drain current	120	*A*
Diodes - FERD40U50C			
V_{RRM}	Repetitive peak reverse voltage	50	*V*
V_F	Forward voltage drop	0.43	*V*
I_F	Average forward current	20	*A*
Secondary side			
C_f	Filtering capacitor	1000	*uF*
R_L	Load value	1 - 50	*Ω*
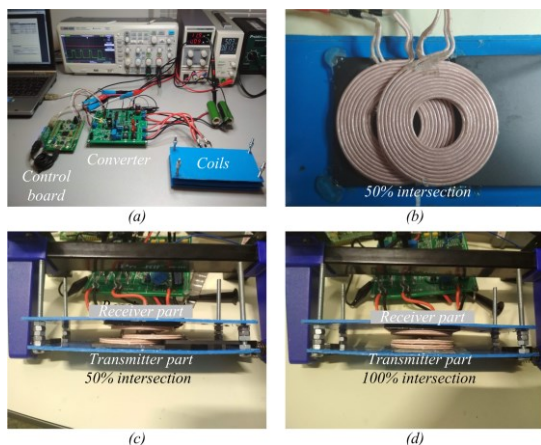
Fig. 8. Testing set: (a) outlook of the components; (b) primary side coils; (c) coils with 50% intersection; (d) coils with 100% intersection.
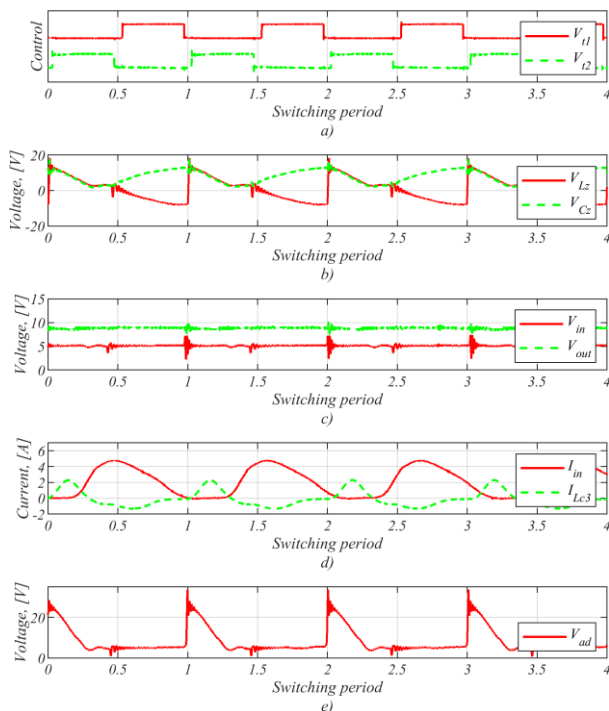

Fig. 9. Experimental results of: (a) control signals; (b) Z-source voltages; (c) output and input voltages; (d) input and receiving coil current; (e) voltage after blocking element.

Fig. 9d shows the secondary coil current, which has the same amplitude and shape as was obtained in the simulation. Measurement equipment adds noise to the input and output voltages, as depicted in Fig. 9c. The boost mode with x2 voltage gain correlates with the simulation results in the previous section.

To compare the solution with the transistor, the blocking diode was replaced on the same board. As was mentioned above, the control signals involve the dead-time between the transistor switching. This time is equal to 5% of the switching period. In this case, no short circuit stages appear in the working mode.

The experimental results were estimated for the load values *10 Ω* and *5 Ω*. Fig. 10 demonstrates the difference in the

efficiency (Fig. 10a) and the voltage gain (Fig. 10b) between the two solutions for coil positions, as shown in Fig. 12b with the air gap and coils alignments ($k_{13} \approx k_{23} \approx 0.35$). As can be seen, the solution that utilizes the transistor gives ~5% increase in the efficiency in the working range and the frequency range of relatively high efficiency was increased (the rapid increase ~40% for the frequencies in the range 60-75 kHz, which corresponds to the Z-source resonance frequency).
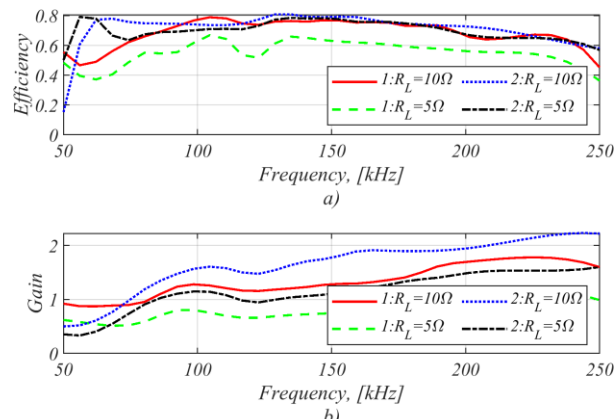

Fig. 10. Experimental results of topologies with the diode (solution 1) and transistor (solution 2): (a) efficiency; (b) voltage gain.

To approximately estimate the losses in the system and identify the elements leading to these losses, the temperature dissipated by the converter was captured for the regular working mode. Fig. 11 shows the results for the topology with one transistor (Fig. 11a) and two transistors (Fig. 11b). On the temperature photos: 1 - the blocking transistor T_1 or diode D_1, 2 – the transistor T_2, 3 – isolated dc-dc converters for the driver supply and 4 – the driver.
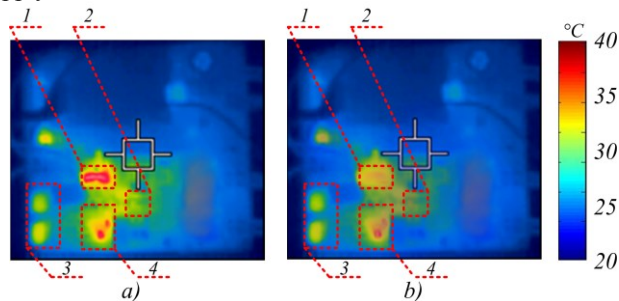

Fig. 11. Photos obtained from the temperature camera for: (a) solution with a diode; (b) solution with a transistor.

To investigate the operation modes based on different transmitting and receiving coil positions, three types of solutions were suggested. In the first solution, the receiver coil is situated between the transmitting coils with the same air gap between each transmitter, as depicted in Fig. 12a. The second solution uses two transmitting coils with 50% misalignments (Fig. 12b) and correspondingly low transmitter coils coupling ($k_{12}<0.05$). The third solution (Fig. 12c) uses an opposite approach. Zero misalignments between the transmitters are used to obtain a high value of coupling between the transmitting coils ($k_{12}>0.95$). It should be noted that in the first two solutions, formula (8) is used to evaluate the values of the

primary side compensation capacitors. The third solution uses formula (6), as it should take into account the mutual inductance of the transmitting coils.

The resulting diagrams of a few switching periods for the proposed solutions are shown in Fig. 12. Input and output voltages and currents (Fig. 12d, Fig. 12e, Fig. 12f) show low noise levels. Only the third solution has a high level of spikes on the input voltages. They occur as the system works at higher power rates than in other solutions. The higher spikes value can be explained by the higher transmitted power than in other solutions.

Overall, the first two solutions show quite similar results for the Z-source part (Fig. 12g, Fig. 12h) and coupled coils part (Fig. 12g, Fig. 12h). Such behavior can be explained by the fact that the only difference of these solutions is in the higher coupling value between the transmitters in the first solution, as they are situated between ferrite shields. The third solution (Fig. 12c) provides a better quality of the transmitted energy. On the other hand, this solution utilizes higher voltage on the Z-source and correspondingly the IPT part. In this case, transistors with a voltage hi1gher than in other solutions should be used in this mode.
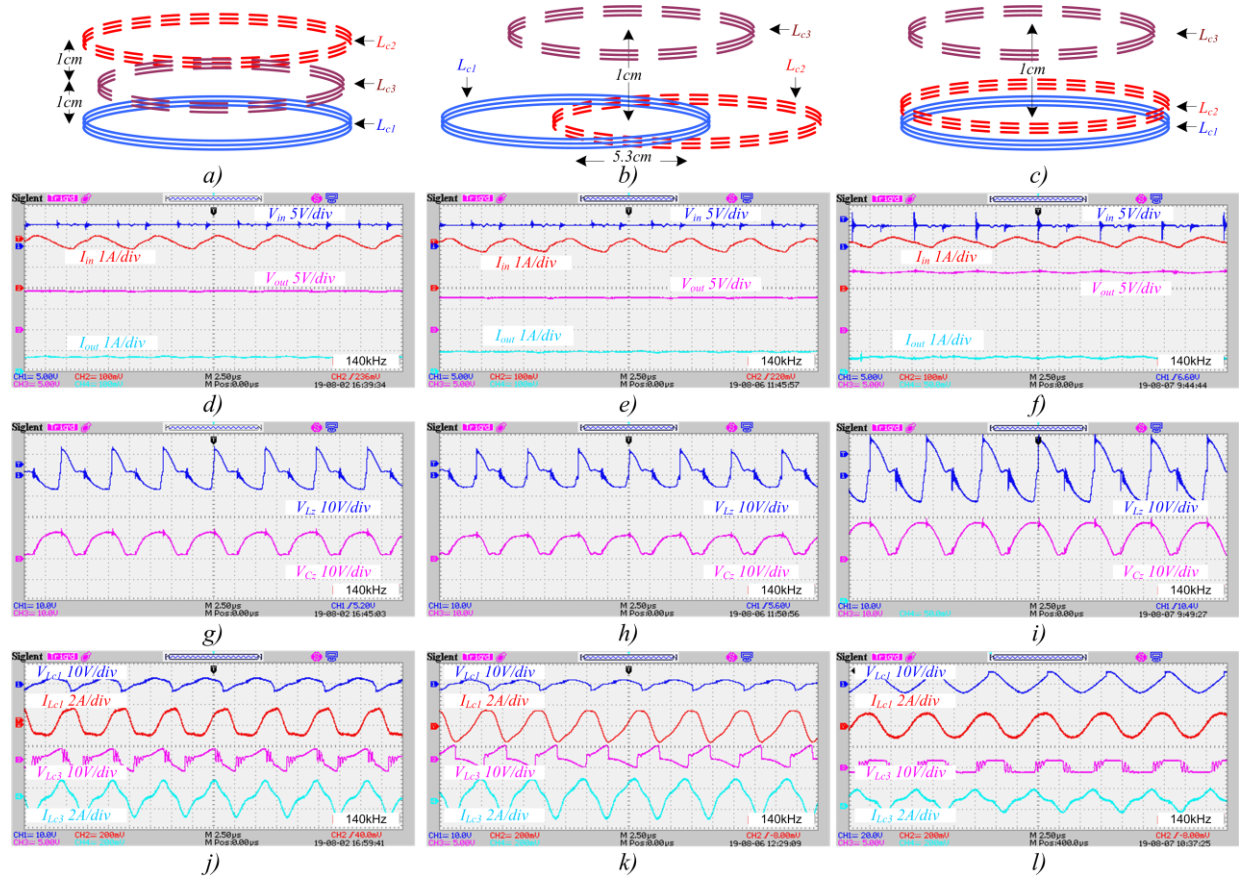

Fig. 12. Results of the proposed solutions: (a) first solution; (b) second solution; (c) third solution; (d) oscillograms of $V_{in}, I_{in}, V_{out}, I_{out}$; (e) oscillograms of $V_{in}, I_{in}, V_{out}, I_{out}$; (f) oscillograms of $V_{in}, I_{in}, V_{out}, I_{out}$; (g) oscillograms of V_{Lz1}, V_{Cz1}; (h) oscillograms of V_{Lz1}, V_{Cz1}; (i) oscillograms of V_{Lz1}, V_{Cz1}; (j) oscillograms of $V_{Lc1}, I_{Lc1}, V_{Lc3}, I_{Lc3}$; (k) oscillograms of $V_{Lc1}, I_{Lc1}, V_{Lc3}, I_{Lc3}$; (l) oscillograms of $V_{Lc1}, I_{Lc1}, V_{Lc3}, I_{Lc3}$.

All the proposed solutions were investigated for different load values (Fig. 13a). Load variation was chosen by the limitation of laboratory power supply, equal to maximum 3.2 A of the input current. The curves show that the optimal load for the first two solutions is approximately the same (*11 Ω* and *8 Ω*) whereas in the third solution, the optimal load is higher (*30 Ω*).

Resulting from the frequency analysis made for the obtained optimal loads (Fig. 13b), the first two solutions are more tolerant to switching frequency changes, while the third solution should use the precise switching frequency, as any frequency deviation would lead to a dramatic efficiency decrease in comparison to the other solutions. This can be explained by the higher quality factor of the resonance circuit in the third solution, which leads to the decreased bandwidth ($BW=f_r/Q$, where f_r-resonance frequency, Q - quality factor).

The efficiency of the different displacements was also analyzed (Fig. 13c). As it was expected, the second solution expanded the effective area significantly. As shown by Fig. 4c, in the first and third solution, the misalignment is larger than a half of the radius; after a zero efficiency point (~3cm), some energy is received from the outer flux of the transmitters.

As the second solution showed the best tolerance to the displacement, its oscillograms were obtained for 1 cm misalignment (Fig. 14). It can be seen that the Z-source elements are not in equilibrium (Fig. 14b and Fig. 14c), as different reflected impedances occurred on each transmitting coil. Nevertheless, due to the availability of compensation elements tuned on the switching frequency, the quality of the transmitted energy still remains high.
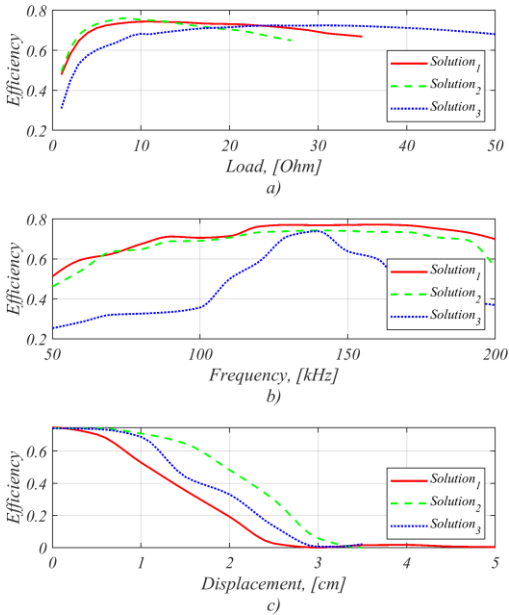
Fig. 13. Efficiency for: (a) different loads; (b) different switching frequencies; (c) different displacements between the transmitter and the receiver.
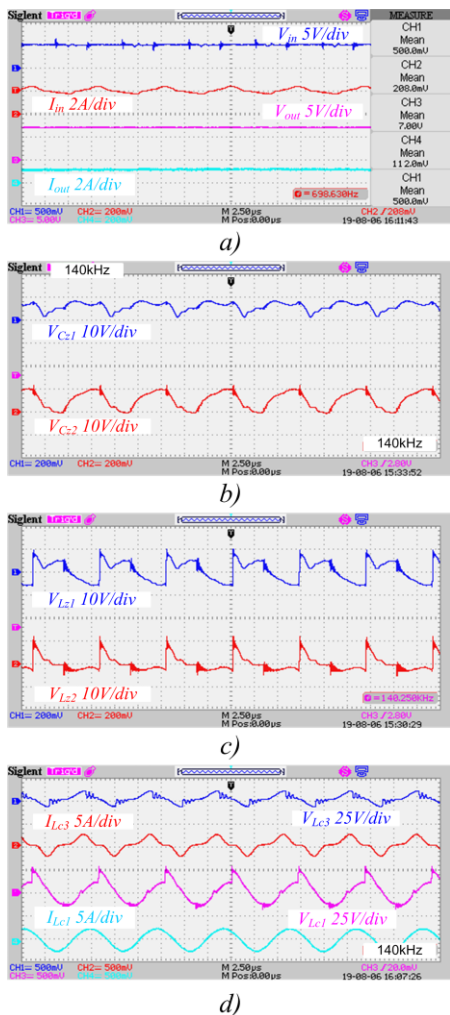

Fig. 14. Results for the second solution with 1 cm coupled coils misalignment: (a) oscillograms of V_{in}, I_{in}, V_{out}, I_{out}; (b) oscillograms of V_{Cz1}, V_{Cz2}; (c) oscillograms of V_{Lz1}, V_{Lz2}; (d) oscillograms of V_{Lc1}, I_{Lc1}, V_{Lc3}, I_{Lc3}.

Finally, by measuring the temperature across semiconductors with passive components and overall efficiency, the losses breakdown was made (Fig. 15). The analysis was performed for coils configuration shown in Fig. 12b. High impact on efficiency was related to Z-source network coils (L_{z1} and L_{z2}). This was caused by usage of non litz-wire inductors, which leads to low quality factor. To decrease level of losses inductors with lower resistance at high frequencies can be used.

The main losses in active elements are related to transistor T_2. This issue cannot be omitted and can be decreased only by using transistors with better parameters.

Despite transistor T_1 is being switched in ZVS mode the valuable impact of losses in caused when body diode of transistor T_1 is conducting. These losses appear in state 3 (Fig. 3.c). As this mode is undesirable it's duration should be minimized. This can be done by make further optimizing of topology for higher reflected impedances. In this case capacitors C_z discharging period (mode 2, Fig. 3.b) can be increased (up to point when capacitors C_z are discharged to vin/2) and lead to decreased duration of state when the body diode conducts.
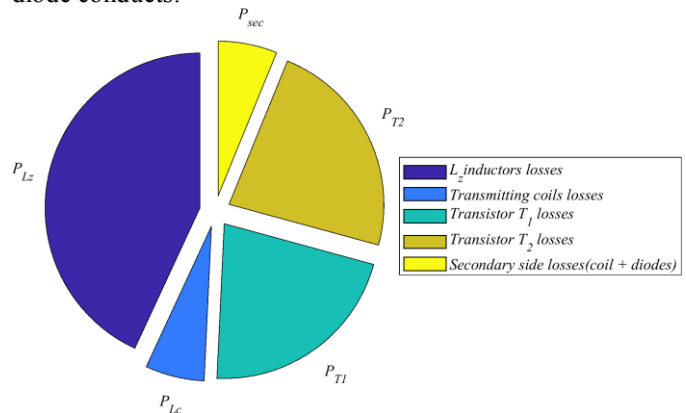

Fig. 15. Losses break down;

Comparison to one of the conventional solutions was performed in advance. For this purpose, an E-class converter with two transmitters was chosen (Fig. 1.d). For a fair comparison, the receiver and the coupled coils circuitry were the same. To satisfy ZVS conditions, component calculation followed the procedure in [63]. As compared to the proposed solution, one additional reactive element should be used (Fig. 1.d). Calculation results show that to obtain ZVS conditions and remove harmonics for approximately the same power rating, as compared to the proposed solution, inductances should be significantly larger. This leads to increased dimensions of the final prototype and increased system tuning complexity. To verify the calculation, an experimental set was designed (Fig. 16). With the same coupled coils, the receiver and the input voltage (5V) (except recalculated secondary compensation capacitor), the efficiency was about 46.5%. As can be seen from Fig. 16, the compensation capacitors of the transmitter and the receiver have sinusoidal voltages, which indicates that the system works under resonant condition and that the channels are symmetrical. The measured voltages across the transistor give evidence that the ZVS conditions are also satisfied.
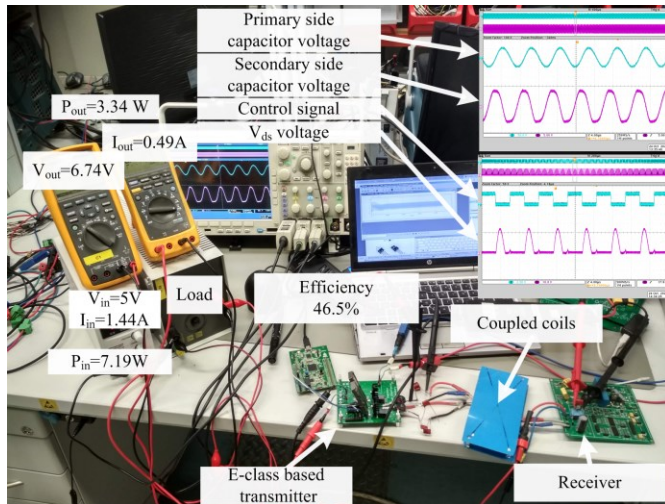
This article has been accepted for publication in a future issue of this journal, but has not been fully edited. Content may change prior to final publication. Citation information: DOI 10.1109/JESTPE.2020.3041565, IEEE Journal of Emerging and Selected Topics in Power Electronics

10

Fig. 16.   Experimental set with an E-class based converter.

CONCLUSIONS

A non-conventional approach of the multi-coils wireless power transfer system based on a Z-source network is presented in this work. It was shown that the Z-source network can be used in a resonance mode as a double voltage source generator. As a result, the multi-coils (double-coils) WPT system can be realized by means of only two semiconductors.

The guidelines for the passive elements selection along with the simulation and experimental verification are provided.

The key advantage of this solution consists in a reduced number of semiconductors. Only two semiconductors are required for two transmitting coils. Two different scenarios of the application are discussed. These scenarios are defined by a mutual location of the primary and secondary side coils. The first scenario assumed a strong coupling of the primary side coils. In this case, the maximum efficiency is expected to be higher. In the second case, the primary side coils are split away, which in turn, slightly deteriorates the maximum efficiency, but improves the efficiency when the secondary side coil is displaced. It means that this solution can be recommended for applications where the secondary side coil can be shifted in a horizontal line.

Finally, despite the simplified experimental prototype with non-optimized semiconductors, the efficiency is acceptable and can be significantly improved by utilizing modern wide band gap semiconductors with minimal dynamic losses.

REFERENCES

[1] S. Bandyopadhyay, P. Venugopal, J. Dong and P. Bauer, "Comparison of Magnetic Couplers for IPT-Based EV Charging Using Multi-Objective Optimization," *IEEE Trans. on Vehicular Techn.*, vol. 68, no. 6, pp. 5416-5429, June 2019.

[2] C. Panchal, S. Stegen, J. Lu, "Review of static and dynamic wireless electric vehicle charging system," *Eng. Sci. Technol. Int. J.* 2018, 21, pp. 922-937.

[3] V. Shevchenko, O. Husev, R. Strzelecki, B. Pakhaliuk, N. Poliakov and N. Strzelecka, "Compensation Topologies in IPT Systems: Standards, Requirements, Classification, Analysis, Comparison and Application," *IEEE Access*, vol. 7, pp. 120559-120580, 2019.

[4] Z. Zhang, H. Pang, A. Georgiadis and C. Cecati, "Wireless Power Transfer—An Overview," *IEEE Transactions on Industrial Electronics*, vol. 66, no. 2, pp. 1044-1058, Feb. 2019.

[5] V. Cirimele, F. Freschi and M. Mitolo, "Inductive power transfer for automotive applications: State-of-the-art and future trends," *in proc. of 2016 IEEE Industry Applications Society Annual Meeting*, Portland, OR, 2016, pp. 1-8.

[6] M.A. Houran, X. Yang, W. Chen, "Magnetically Coupled Resonance WPT: Review of Compensation Topologies, Resonator Structures with Misalignment, and EMI Diagnostics," *Electronics* 2018, 7, 296.

[7] S. Huh, D. Ahn, "Two-Transmitter Wireless Power Transfer with Optimal Activation and Current Selection of Transmitters," *IEEE Trans. on Power Electron.*, vol. 33, no. 6, pp. 4957-4967, June 2018.

[8] Y. Liu, B. Li, M. Huang, Z. Chen, X. Zhang, "An Overview of Regulation Topologies in Resonant Wireless Power Transfer Systems for Consumer Electronics or Bio-Implants," *Energies* 2018, 11, 1737.

[9] `D. Patil, M. K. McDonough, J. M. Miller, B. Fahimi and P. T. Balsara, "Wireless Power Transfer for Vehicular Applications: Overview and Challenges," *IEEE Trans. on Transportation Electrification*, vol. 4, no. 1, pp. 3-37, March 2018.

[10] S. Y. R. Hui, W. Zhong and C. K. Lee, "A Critical Review of Recent Progress in Mid-Range Wireless Power Transfer," *IEEE Trans. on Power Electron.*, vol. 29, no. 9, pp. 4500-4511, Sept. 2014.

[11] R. Saltanovs, A. Krivchenkov, A. Krainyukov "Analysis of effective wireless communications for V2G applications and mobile objects," in *proc. of 58th International Scientific Conference on Power and Electrical Engineering of Riga Technical University*, 2017, pp. 1-5.

[12] R. Saltanovs, I. Galkin, "Method of adjustment and stabilization of parameters for wireless energy transfer system.Proceedings" in *proc. of 19th European Conference on Power Electronics and Applications*, 2017, pp. 1-6.

[13] O. Knecht and J. W. Kolar, "Comparative evaluation of IPT resonant circuit topologies for wireless power supplies of implantable mechanical circulatory support systems," in *proc. of 2017 IEEE Applied Power Electronics Conference and Exposition (APEC)*, Tampa, FL, 2017, pp. 3271-3278.

[14] J. Bito, S. Jeong and M. M. Tentzeris, "A Real-Time Electrically Controlled Active Matching Circuit Utilizing Genetic Algorithms for Wireless Power Transfer to Biomedical Implants," *IEEE Trans. on Microwave Theory and Techniques*, vol. 64, no. 2, pp. 365-374, Feb. 2016.

[15] O. Knecht, R. Bosshard, J. W. Kolar and C. T. Starck, "Optimization of Transcutaneous Energy Transfer coils for high power medical applications," in *proc. of 2014 IEEE 15th Workshop on Control and Modeling for Power Electronics (COMPEL)*, Santander, 2014, pp. 1-10.

[16] Z. Zhang, W. Ai, Z. Liang and J. Wang, "Topology-Reconfigurable Capacitor Matrix for Encrypted Dynamic Wireless Charging of Electric Vehicles," *IEEE Trans. on Vehicular Techn.*, vol. 67, no. 10, pp. 9284-9293, Oct. 2018.

[17] T. Kan, T. Nguyen, J. C. White, R. K. Malhan and C. C. Mi, "A New Integration Method for an Electric Vehicle Wireless Charging System Using LCC Compensation Topology: Analysis and Design," *IEEE Trans. on Power Elec.*, vol. 32, no. 2, pp. 1638-1650, Feb. 2017.

[18] Z. Huang, S. Wong and C. K. Tse, "Design of a Single-Stage Inductive-Power-Transfer Converter for Efficient EV Battery Charging," *IEEE Trans. on Vehicular Techn.*, vol. 66, no. 7, pp. 5808-5821, July 2017.

[19] K. Hata, T. Imura and Y. Hori, "Dynamic wireless power transfer system for electric vehicles to simplify ground facilities - power control and efficiency maximization on the secondary side," in *proc. of 2016 IEEE Applied Power Electronics Conference and Exposition (APEC)*, Long Beach, CA, 2016, pp. 1731-1736.

[20] Y. Chen, H. Zhang, S. J. Park, D.H. Kim, "A Comparative Study of S-S and LCCL-S Compensation Topologies Inductive Power Transfer Systems for Electric Vehicles," *Energies* 2019, 12, 1913.

[21] V. B. Vu, V. T. Doan, V. L. Pham and W. Choi, "A new method to implement the constant Current-Constant Voltage charge of the Inductive Power Transfer system for Electric Vehicle applications," in *proc. of 2016*

This article has been accepted for publication in a future issue of this journal, but has not been fully edited. Content may change prior to final publication. Citation information: DOI 10.1109/JESTPE.2020.3041565, IEEE Journal of Emerging and Selected Topics in Power Electronics

11

IEEE Transportation Electrification Conference and Expo, Asia-Pacific (ITEC Asia-Pacific), Busan, 2016, pp. 449-453.

[22] D. H. Tran, V. B. Vu and W. Choi, "Design of a High-Efficiency Wireless Power Transfer System With Intermediate Coils for the On-Board Chargers of Electric Vehicles," *IEEE Trans. on Power Elec.*, vol. 33, no. 1, pp. 175-187, Jan. 2018.

[23] R. Bosshard and J. W. Kolar, "Inductive power transfer for electric vehicle charging: Technical challenges and tradeoffs," *IEEE Power Electronics Magazine*, vol. 3, no. 3, pp. 22-30, Sept. 2016.

[24] Z. Yan et al., "Frequency Optimization of a Loosely Coupled Underwater Wireless Power Transfer System Considering Eddy Current Loss," *IEEE Trans. on Industrial Elec.*, vol. 66, no. 5, pp. 3468-3476, May 2019.

[25] A. Askari, R. Stark, J. Curran, D. Rule and K. Lin, "Underwater wireless power transfer," in *proc. of 2015 IEEE Wireless Power Transfer Conference (WPTC)*, Boulder, CO, 2015, pp. 1-4.

[26] D. Futagami, Y. Sawahara, T. Ishizaki and I. Awai, "Study on high efficiency WPT underseas," in *proc. of 2015 IEEE Wireless Power Transfer Conference (WPTC)*, Boulder, CO, 2015, pp. 1-4.

[27] J. Oiler, G. Anderson, V. Bana, A. Phipps, M. Kerber and J. D. Rockway, "Thermal and biofouling effects on underwater wireless power transfer," in *proc. of 2015 IEEE Wireless Power Transfer Conference (WPTC)*, Boulder, CO, 2015, pp. 1-4.

[28] K. Kroics, J. Voitkans and B. Pakhaliuk, "Design Considerations of GaN Transistor Based Capacitive Wireless Power Transfer System," in *proc. of 2018 IEEE 18th International Power Electronics and Motion Control Conference (PEMC)*, Budapest, 2018, pp. 66-71.

[29] V. Vu et al., "A multi-output capacitive charger for electric vehicles," in *proc. of 2017 IEEE 26th International Symposium on Industrial Electronics (ISIE)*, Edinburgh, 2017, pp. 565-569.

[30] Z. Huang, S. Wong and C. K. Tse, "An Inductive-Power-Transfer Converter With High Efficiency Throughout Battery-Charging Process," *IEEE Trans. on Power Elec.*, vol. 34, no. 10, pp. 10245-10255, Oct. 2019.

[31] Z. Huang, S. Wong and C. K. Tse, "Design of a Single-Stage Inductive-Power-Transfer Converter for Efficient EV Battery Charging," *IEEE Trans. on Vehicular Techn.*, vol. 66, no. 7, pp. 5808-5821, July 2017.

[32] N. Inagaki, "Theory of Image Impedance Matching for Inductively Coupled Power Transfer Systems," *IEEE Trans. on Microwave Theory and Techniques*, vol. 62, no. 4, pp. 901-908, April 2014.

[33] M. P. Kazmierkowski, R. M. Miskiewicz and A. J. Moradewicz, "Inductive coupled contactless energy transfer systems - a review," in *proc. of 2015 Selected Problems of Electrical Engineering and Electronics (WZEE)*, Kielce, 2015, pp. 1-6.

[34] Wireless Power Consortium, "Qi system description: Wireless power transfer," vol. I: Low Power, Part 1: Interface Definition, Version 1.1, April 2012.

[35] R. Tseng, B. von Novak, S. Shevde and K. A. Grajski, "Introduction to the Alliance for Wireless Power Loosely-coupled Wireless Power Transfer System Specification Version 1.0," in *proc. of IEEE Wireless Power Transfer (WPT)*, Perugia, Italy, May 2013.

[36] M. Leibl, O. Knecht and J. W. Kolar, "Inductive Power Transfer Efficiency Limit of a Flat Half-Filled Disc Coil Pair," *IEEE Trans. on Power Elec.*, vol. 33, no. 11, pp. 9154-9162, Nov. 2018.

[37] R. Bosshard, J. W. Kolar, J. Mühlethaler, I. Stevanović, B. Wunsch and F. Canales, "Modeling andη-α-Pareto Optimization of Inductive Power Transfer Coils for Electric Vehicles," *IEEE Journal of Emerging and Selected Topics in Power Electronics*, vol. 3, no. 1, pp. 50-64, March 2015.

[38] X. Dai, J. Jiang, Y. Li, T. Yang, "A Phase-Shifted Control for Wireless Power Transfer System by Using Dual Excitation Units," *Energies* 2017, 10, 1000.

[39] F. Lin, G. A. Covic and J. T. Boys, "A Comparison of Multi-Coil Pads in IPT systems for EV Charging," in *proc. of 2018 IEEE Energy Conversion Congress and Exposition (ECCE)*, Portland, OR, 2018, pp. 105-112.

[40] J. Zhang, X. Yuan, C. Wang, Y. He,. "Comparative Analysis of Two-Coil and Three-Coil Structures for Wireless Power Transfer". *IEEE Trans. on Power Elec.*, 32(1), 341–352, 2017.

[41] Y. Cao and J. A. A. Qahouq, "Analysis and evaluation of input power splitting method between multiple transmitters for maximum wireless power transfer," in *proc. of IEEE Applied Power Electronics Conference and Exposition (APEC)*, San Antonio, 2018, pp. 959-962.

[42] T. Arakawa et al., "Optimizing Wireless Power Transfer From Multiple Transmit Coils," *IEEE Access*, vol. 6, pp. 23828-23838, 2018.

[43] V. Vu, V. Phan, M. Dahidah and V. Pickert, "Multiple Output Inductive Charger for Electric Vehicles," *IEEE Trans. on Power Elec.*, vol. 34, no. 8, pp. 7350-7368, 2019.

[44] C. Anyapo, N. Teerakawanich and C. Mitsantisuk, "Development of multi-coils full-bridge resonant inverter for dynamic wireless power transfer," in *proc. of 2017 14th International Conference on Electrical Engineering/Electronics, Computer, Telecommunications and Information Technology (ECTI-CON)*, Phuket, 2017, pp. 588-591.

[45] F. Faradjizadeh, M. Vilathgamuwa, D. Jovanovic, P. Jayathurathnage, G. Ledwich and U. Madawala, "Expandable N-Legged Converter to Drive Closely Spaced Multi Transmitter Wireless Power Transfer Systems for Dynamic Charging," *IEEE Transactions on Power Electronics*.

[46] T. Marojahan, P. Laskar, and C. Huang-Jen, "Dynamic wireless power transfer for logistic robots," *Energies*, vol. 11, no. 3, pp. 527, 2018.

[47] X. Ge, Y. Sun, Z. Wang and C. Tang, "Dual-Independent-Output Inverter for Dynamic Wireless Power Transfer System," *IEEE Access*, vol. 7, pp. 107320-107333, 2019.

[48] S. Y. Jeong, J. H. Park, G. P. Hong and C. T. Rim, "Autotuning Control System by Variation of Self-Inductance for Dynamic Wireless EV Charging With Small Air Gap," *IEEE Transactions on Power Electronics*, vol. 34, no. 6, pp. 5165-5174

[49] D. Patil, M. Sirico, L. Gu and B. Fahimi, "Maximum efficiency tracking in wireless power transfer for battery charger: Phase shift and frequency control," in *proc. of 2016 IEEE Energy Conversion Congress and Exposition (ECCE)*, Milwaukee, 2016, pp. 1-8.

[50] S. Judek and K. Karwowski, "Analysis of inductive power transfer systems for variable air gap and voltage supply frequency," in *proc. of IEEE International Symposium on Industrial Electronics*, Gdansk, 2011, pp. 1963-1968.

[51] Y. Liu and H. Feng, "Maximum Efficiency Tracking Control Method for WPT System Based on Dynamic Coupling Coefficient Identification and Impedance Matching Network," *IEEE Journal of Emerging and Selected Topics in Power Electronics*.

[52] Chaoqiang Jiang, K. T. Chau, Chunhua Liu, Christopher H. T. Lee, "An Overview of Resonant Circuits for Wireless Power Transfer," Energies 2017, 10(7), 894.

[53] F. Z. Peng, "Z-source inverter," *IEEE Trans. Ind. Appl.*, vol. 39, no. 2, pp. 504–510, Mar./Apr. 2003.

[54] N. S. González-Santini, H. Zeng, Y. Yu and F. Z. Peng, "Z-Source Resonant Converter With Power Factor Correction for Wireless Power Transfer Applications," *IEEE Trans. on Power Elec.*, vol. 31, no. 11, pp. 7691-7700, Nov. 2016.

[55] W. Tianfeng, L. Xin, T. Houjun, D. Yayun and Y. Xijun, "Modeling and advanced control of wireless power transfer system with Z-source inverter," in *proc. of 2016 IEEE 2nd Annual Southern Power Electronics Conference (SPEC)*, Auckland, 2016, pp. 1-6.

[56] H. Zeng and F. Z. Peng, "SiC-Based Z-Source Resonant Converter With Constant Frequency and Load Regulation for EV Wireless Charger," *IEEE Trans. on Power Elec.*, vol. 32, no. 11, pp. 8813-8822, Nov. 2017.

[57] L. Huang, A. P. Hu, A. K. Swain and Y. Su, "Z-Impedance Compensation for Wireless Power Transfer Based on Electric Field," *IEEE Trans. on Power Elec.*, vol. 31, no. 11, pp. 7556-7563, Nov. 2016.

[58] B. Pakhaliuk, O. Husev, V. Shevchenko, O. Veligorskyi and K. Kroics, "Novel Inductive Power Transfer Approach Based on Z-Source Network with Compensation Circuit," in *proc. of 2018 IEEE 38th International Conference on Electronics and Nanotechnology (ELNANO)*, Kiev, 2018, pp. 699-704.

[59] B. Pakhaliuk, O. Husev, R. Strzelecki and K. Tytelmaier, "Optimal Components Design for Modified Z-Source Based IPT Approach," in *proc. of 2018 IEEE 3rd International Conference on Intelligent Energy and Power Systems (IEPS)*, Kharkiv, 2018, pp. 11-16.

[60] K. Kroics, O. Husev, B. Pakhaliuk, J. Zakis, O. Velihorskyi and R. Strzelecki, "Single Switch Multi-Winding Wireless Power Transfer System Based on Z-Source Network," in *proc. of 2018 20th European*

This article has been accepted for publication in a future issue of this journal, but has not been fully edited. Content may change prior to final publication. Citation information: DOI 10.1109/JESTPE.2020.3041565, IEEE Journal of Emerging and Selected Topics in Power Electronics

12

Conference on Power Electronics and Applications (EPE'18 ECCE Europe), Riga, 2018, pp.1-9.

[61] X. Dai, J. Jiang, Y. Li, T. Yang, "A Phase-Shifted Control for Wireless Power Transfer System by Using Dual Excitation Units," *Energies* 2017, 10, 1000.

[62] R. W. Erickson and D. Maksimovic, "A multiple-winding magnetics model having directly measurable parameters," in *proc. of PESC 98 Record. 29th Annual IEEE Power Electronics Specialists Conference (Cat. No.98CH36196)*, Fukuoka, 1998, pp. 1472-1478 vol.2.

[63] F. Corti, F. Grasso, A. Reatti, A. Ayachit, D. K. Saini and M. K. Kazimierczuk, "Design of class-E ZVS inverter with loosely-coupled transformer at fixed coupling coefficient," in *proc. of IECON 2016 - 42nd Annual Conference of the IEEE Industrial Electronics Society*, Florence, 2016.
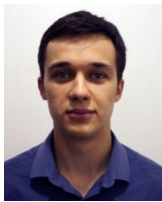
Bohdan Pakhaliuk (S`18) received the B.Sc. and M.Sc. degrees in industrial electonics from Chernihiv National University of Technology, Chernihiv, Ukraine, in 2016 and 2018 respectively. He is PhD student of double postgraduate study, in Gdansk University of Technology and Chernihiv Polytechnic National University. He is junior researcher of the Chernihiv power electronics laboratory, Chernihiv Polytechnic National University and Linte2 laboratory, Gdansk University of Technology. His research interests are, design and control of converters for wireless power transfer applications.
E-mail:bohdan.pakhaliuk@ieee.org, bohdan.pakhaliuk@gmail.com

Oleksandr Husev (S'10–M'12-SM'19) received the B.Sc. and M.Sc. degrees in industrial electronics from Chernihiv State Technological University, Chernihiv, Ukraine, in 2007 and 2008 respectively. He defended PhD thesis in the Institute of Electrodynamics of the National Academy of Science of Ukraine in 2012.
He is senior researcher of the Department of Electrical Power Engineering and Mechatronics, TalTech University He has over 100 publications and is the holder of several patents.
His research interests are in Power Electronics systems. Design of novel topologies, control systems based on a wide range of algorithms, including modeling, design, and simulation. Applied design of power converters and control systems and application, stability investigation.
E-mail: oleksandr.husev@ieee.org

Viktor Shevchenko (S'18) was born in 1990, Ukraine. He received the B.Sc. and M.Sc. degrees in industrial electronics from Chernihiv National University of Technology, Chernihiv, Ukraine, in 2015 and 2017 respectively. He became PhD student in 2017. He is junior researcher and teacher's assistant of the Radiotechnic and Embedded Systems Department, Chernihiv Polytechnic National University. He has several publications and patents. His area of research interests includes power electronics systems, wireless power transfer, photovoltaic systems.
E-mail: shevaip1990@gmail.com

Janis. Zakis (M10 - SM14) received B. Sc., M Sc. and Dr. sc. ing. in electrical engineering from Riga Technical University, Riga, Latvia, in 2002, 2004 and 2008, respectively. He is curently a Senior Researcher with the Institute of Industrial Electronics and Electrical Engineering, Riga Technical University. He has over 75 publications in journals and conference proceedings and is the holder of several patents.
E-mail: janis.zakis@rtu.Iv, janis.zakis@ieee.org

Maksym Khomenko received his B.S. in Electronics and M.S in Electronic Systems from Chernihiv State University of Technology (CSUT), Chernihiv, Ukraine, in 2003 and 2004 respectively, his PhD in Electrical Engineering from National Technical University of Ukraine "Kyiv Politechnic Institute" in 2011. He became an Engineer in 2004, a lecturer in 2008, and Associate Professor in 2012 at Chernihiv National University of Technology. Since 2017 to 2018 he was working as research fellow in Bonn-Rhein-Sieg University of Applied Sciences. His current research interests include intelligent control systems, artificial neural networks, signal processing, power electronics and renewable energy.
E-mail: mr.homax@gmail.com

Ryszard Strzelecki (S'11–M'23) graduated from Industrial Electronics at the Kyiv Polytechnic Institute in 1981. In 1984 he received Ph.D. degree and in 1991 he passed habilitation (D.Sc.). In 1999, he received the title of professor of technical sciences. His interests focus on topologies and control methods as well as industrial application of power electronic systems. Currently, he is full professor at Gdansk University of Technology (Poland), and co-Head with the Laboratory of Power Electronics and Automated Electric Drive, ITMO University (St. Petersburg, Russia), and Researsch Consultant at AREX Ltd (Gdynia, Poland)
E-mail: ryszard.strzelecki@pg.edu.pl